Invasion percolation with long-range correlations: First-order phase transition and nonuniversal scaling properties

Mark A. Knackstedt,[1,2] Muhammad Sahimi,[3,*] and Adrian P. Sheppard[1,2]
[1]*Department of Applied Mathematics, Research School of Physical Sciences and Engineering, Australian National University, Canberra ACT 0200, Australia*
[2]*Australian Petroleum Cooperative Research Centre, University of New South Wales, Sydney, NSW 2052, Australia*
[3]*Department of Chemical Engineering, University of Southern California, Los Angeles, California 90089-1211*
(Received 16 November 1999)

We present the results of extensive Monte Carlo simulations of the invasion percolation model with trapping (TIP) with long-range correlations, a problem which is relevant to multiphase flow in field-scale porous media, such as oil reservoirs and groundwater aquifers, as well as flow in rock fractures. The correlations are generated by a fractional Brownian motion characterized by a Hurst exponent H. We employ a highly efficient algorithm for simulating TIP, and a novel method for identifying the backbone of TIP clusters. Both site and bond TIP are studied. Our study indicates that the backbone of bond TIP is loopless and completely different from that of site TIP. We obtain precise estimates for the fractal dimensions of the sample-spanning cluster (SSC), the minimal path, and the backbone of site and bond TIP, and analyze the size distribution of the trapped clusters, in order to identify all the possible universality classes of TIP with long-range correlations. For site TIP with $H>1/2$ the SSC and its backbone are *compact*, indicating a first-order phase transition at the percolation threshold, while the minimal paths are essentially straigth lines. For $H<1/2$ the SSC, its backbone, and the minimal paths are all fractal with fractal dimensions that depend on the Hurst exponent H. The fractal dimension of the loopless backbone for bond TIP is much less than that of site TIP for any H.

PACS number(s): 64.60.Ak, 47.55.Mh

I. INTRODUCTION

Multiphase flow phenomena in porous media are relevant to many problems of great scientific and industrial importance, including extraction of oil, gas, and geothermal energy from underground reservoirs, and transport of contaminants in soils and aquifers. To investigate these phenomena, pore network models have been used to represent the porous media, and the concepts of percolation theory [1–3] have been employed to model slow flow of fluids through the pore space. These models include both random bond or site percolation [4–9] and invasion percolation (IP) [10–12]. In particular, IP, which was introduced for describing the evolution of the interface between an invading and a defending fluid in a porous medium, has provided deep insight into such phenomena. In addition, IP is relevant to a host of other problems, including characterization of optimal paths and domain walls in strongly disordered media [13,14], and even simulation of the Ising model at the critical temperature [15]. Moreover, IP is one of the simplest parameter-free models, which exhibits self-organized criticality [16], another subject of current interest.

Two different variants of IP, both motivated by the physics of multiphase flow in porous media, have been studied so far. In one the defending fluid is infinitely compressible and the invading fluid can potentially enter any region on the interface that is occupied by the defending fluid. We refer to this as the nontrapping IP (NTIP). In the second and more common model, the defending fluid is incompressible and can be trapped if a portion of it is surrounded by the invading fluid. We call this the trapping IP (TIP). The fluids' compressibility is, however, only one of several factors that affect the evolution of the system as the invading fluid advances in the porous medium. In particular, one must also take into account the ability of the fluids to wet the internal surface of the medium [1]. The process by which a wetting fluid is drawn spontaneously into a porous medium is called imbibition, while forcing of a nonwetting fluid into the pore space is called drainage. We model the porous medium as a network of pores or sites connected by throats or bonds that have smaller radii than the pores. In IP, the potential displacement events are ranked according to the capillary pressure threshold that must be exceeded before a given event takes place. During imbibition, the invading fluid is drawn first into the smallest constrictions, for which the capillary pressure is large and negative, and it goes last into the widest pores. Displacement events are therefore ranked in terms of the largest opening that the invading fluid must travel through, since it is from these larger capillaries that it is most difficult to displace the defender. Imbibition is therefore a *site* IP and, by contrast, drainage in which the invader has most difficulty with the smallest constrictions, is a *bond* IP.

Important differences arise in the structure of the invading fluids' paths depending on whether one considers NTIP or TIP. Moreover, the question of the universality class of IP has recently been studied extensively [14,17,18]. The scaling properties of NTIP are believed to be consistent with those of random percolation (RP). For TIP the fractal dimension D_f of the sample-spanning cluster (SSC) in two dimensions (2D) is smaller than that of RP [10]. In 3D no significant difference between the fractal dimensions of the SSC for TIP

*Author to whom correspondence should be addressed. Electronic address: moe@iran.usc.edu

and RP has been reported. It was originally argued [10] that the fractal properties of IP, e.g., the fractal dimension of the SSC at the breakthrough point (i.e., at the point where the invading fluid first spans the network) do not depend on whether one simulates a site or bond IP. Recently, however, it was argued [14,18] that important differences arise in the structure of the invading fluid's paths when comparing site and bond IP. Porto *et al.* [14] used a mapping from the minimal (shortest) paths in TIP to the optimal paths in strongly disordered media, and presented numerical evidence that for TIP the fractal dimension D_{min} of the minimal path in all dimensions is not the same as that of RP, and hence they argued that TIP and RP do not belong to the same universality class. On the other hand, Barabási [19] argued that the loopless bond TIP (see below) is in the universality class of RP. It now appears that [20] in 2D IP is characterized by *two* universality classes, one each for NTIP, and site and bond TIP, while in 3D site NTIP and TIP are in the universality class of RP, and (similar to 2D) bond TIP is in the universality class of optimal paths in strongly disordered media.

However, most of the IP processes that have been studied so far deal with systems in which there is no correlation. The nature of disorder in many important classes of disordered porous media is not, however, completely random, and there usually are correlations of a given extent. However, the scaling properties of percolation models with finite-range correlations are the same as those of RP, if the length scale of interest is larger than the correlation length. Moreover, if the correlation function decays faster than r^{-d}, where r is the distance between two points and d is the dimensionality of the system, then the critical properties of the systems are identical with those of RP [2,3]. In some other cases, e.g., field-scale porous media and aquifers, there are long-range correlations (see below) whose extent is the same as, or comparable with, the linear size of the system.

In the past, several papers have dealt with percolation with long-range correlations [21–24]. For example, Weinrib and Halperin [22] considered the case for which the correlation function $C(r)$ defined by $C(r)=\langle u(r')u(r+r')\rangle$, where $u(r)$ is a stochastic variable following a distribution with long-range correlations, and $\langle\ \rangle$ denotes an average over all values of r', was given by

$$C(r)\sim r^{-\lambda}, \tag{1}$$

where $\lambda<d$. They calculated the critical exponents of this percolation model to linear order in $\epsilon=6-d$ and $\delta=4-\lambda$, and found them to be nonuniversal and dependent on λ. Prakash *et al.* [24] considered a slightly different percolation model in which the correlation function in a d-dimensional system was given by

$$C(r)\sim r^{-(d-\zeta)}, \tag{2}$$

where $-2\leqslant\zeta\leqslant 2$ is a parameter such that $0\leqslant\zeta\leqslant 2$ represents positive correlations, while $-2\leqslant\zeta\leqslant 0$ corresponds to negative correlations. They studied this model in 2D and argued that the fractal dimension D_f of the SSC is the same as that of RP, while other critical exponents of their model were nonuniversal and dependent on ζ.

Equations (1) and (2) describe systems in which the correlations *decrease* with increrasing r. As discussed in Ref. [25], percolation with long-range correlations in which $C(r)$ *increases* with increasing r is completely different from those characterized by Eq. (1) or (2). One stochastic process with a correlation function that increases with r is the fractional Brownian motion $B_H(\mathbf{r})$ (FBM) [26], which has the properties that $\langle B_H(\mathbf{r})-B_H(\mathbf{r}_0)\rangle=0$, and

$$\langle[B_H(\mathbf{r})-B_H(\mathbf{r}_0)]^2\rangle\sim|\mathbf{r}-\mathbf{r}_0|^{2H}, \tag{3}$$

where $\mathbf{r}=(x,y,z)$ and $\mathbf{r}_0=(x_0,y_0,z_0)$ are two arbitrary points, and H is the Hurst exponent. A remarkable property of FBM is that it generates correlations whose extent is *infinite*, by which we mean the extent of the correlations is as large as the linear size of the system. Moreover, the type of correlations can be tuned by varying H. If $H>1/2$, then FBM displays persistence, i.e., a trend (for example, a high or low value) at x is likely to be followed by a similar trend at $x+\Delta x$. If $H<1/2$, then FBM generates antipersistence, i.e., a trend at x is not likely to be followed by a similar trend at $x+\Delta x$. For $H=1/2$ the trace of FBM is similar to that of a random walk, and its increments are uncorrelated. The power spectrum $S(\boldsymbol{\omega})$ of a d-dimensional FBM is given by

$$S(\boldsymbol{\omega})=\frac{a_d}{\left(\sum_{i=1}^{d}\omega_i^2\right)^{H+d/2}}, \tag{4}$$

where a_d is a constant, and $\boldsymbol{\omega}=(\omega_1,\ldots,\omega_d)$. This spectral representation also allows us to introduce a cutoff length scale $\ell_{co}=1/\sqrt{\omega_{co}}$ such that

$$S(\boldsymbol{\omega},\omega_{co})=\frac{a_d}{\left(\omega_{co}+\sum_{i=1}^{d}\omega_i^2\right)^{H+d/2}}. \tag{5}$$

By tuning the cutoff length scale one can control the length scale over which the spatial properties of a system are correlated (or anticorrelated). Hence, for length scales $\ell<\ell_{co}$ they preserve their correlations (anticorrelations), but for $\ell>\ell_{co}$ they become random and uncorrelated. Note that for FBM

$$C(r)-C(0)\sim r^{2H}. \tag{6}$$

Since only $H>0$ are physically interesting, for FBM $C(r)$ increases as r does. The spectral representation also provides a convenient method for generating a d-dimensional array of numbers that follow the statistics of FBM. An alternative algorithm for simulating FBM, based on its integral representation, is described by Rambaldi and Pinazza [27].

A percolation model in which the long-range correlations were generated by a FBM was first proposed by Sahimi [28]. The motivation for his model was provided by the work of Hewett [29], who analyzed the permeability distributions and porosity logs of heterogeneous rock formations at large length scales (of order of hundreds of meters), and showed that the porosity logs in the direction perpendicular to the bedding follows the statistics of fractional Gaussian noise (FGN) which is, roughly speaking, the numerical derivative of FBM, while those parallel to the bedding follow the FBM.

In addition, there is convincing evidence that the permeability distribution of many oil reservoirs [1,29] and aquifers [30] can be described by FBM. In Sahimi's model, one first generates a *d*-dimensional FBM array using a lattice and assigns the resulting correlated numbers to the bonds or sites of the lattice. To construct a percolation model and to preserve the correlations between the bonds (sites), one removes those bonds (sites) that have been assigned the *smallest* FBM-generated numbers. We refer to this version of the percolation model with long-range correlations as the standard percolation (SP) model. Over the past few years, these types of percolation models have been studied by a few research groups [28,31,32]. Mourzenko *et al.* [33] used this type of model to study conduction in network of fractures with long-range correlations that were generated by a FBM, while, using a somewhat similar model, Wagner *et al.* [34] studied invasion of a single fracture.

However, since IP is a more appropriate model than the SP for studying multiphase flow in porous media, and because field-scale porous media are typically characterized by FBM- or FGN-type of long-range correlations, in order to describe multiphase flow in such media one must study IP in which the correlations are generated by a FBM (or FGN). Knackstedt *et al.* [35] already used such a model to study mercury porosimetry in correlated porous media, an important process that is used for characterizing the pore structure of a porous medium. The goal of this paper is to report the results of such an investigation. We are particularly interested in the fractal properties of the IP model with long-range correlations, as they may shed light on the nature of multiphase flow phenomena in field-scale porous media.

The plan of this paper is as follows. In Sec. II we describe the TIP model that we study in this paper. An important aspect of studying any IP model is an efficient simulation algorithm, so that large lattices can be used. Thus, we describe in Sec. III the algorithms that we used in our study. In Sec. IV we describe how the simulation results are analyzed, while the results are presented and discussed in Sec. V. Finally, Sec. VI summarizes the paper.

II. INVASION PERCOLATION WITH LONG-RANGE CORRELATIONS

We now describe the TIP model with long-range correlations that are generated by the FBM. We first generate a *d*-dimensional FBM array and assign the resulting numbers to the sites (or bonds) of the *d*-dimensional lattice. The FBM array can be generated either by the methods mentioned above, or by the successive random addition method of Voss [36]; we used the latter method. The FBM-generated numbers are then taken as the effective radii (or permeabilities that are proportional to the square of their radii) of the sites or bonds. The simulation of IP in this lattice is then the same as in the standard TIP, namely, at each time step during invasion, the invading fluid attempts to invade the interface site with the largest number. To investigate the effect of a finite correlation length on the results, we also introduce the cutoff length scale ℓ_{co} (see above) and study its effect on the fractal properties of TIP. In the discussions below the cutoff length scale ℓ_{co} is measured in units of the lattice bonds.

We also studied a variant of TIP, namely, the bond TIP which is more appropriate for modelling invasion of a porous medium by a nonwetting fluid. In essence, if the nonwetting fluid is about to enter a new site that has two neighboring bonds, filled with the wetting fluid, with end sites that are filled with the nonwetting fluid, then the invading fluid breaks through the larger of the two bonds. The smaller bond still contains the wetting fluid and is therefore effectively trapped by its two end sites filled with the nonwetting fluid. To simulate the bond TIP, the FBM-generated numbers are assigned to the bonds of the lattice rather than its sites, and the invading fluid always invades the largest bond at the interface with the defending fluid. This version of TIP generates clusters that are loopless [13,14,17,18].

One of the most essential aspects of studying TIP is having a highly efficient algorithm for simulation of the invasion process. In this work we used the invasion algorithm recently introduced by us [20,37]. Since we also study the backbone of the invasion cluster, i.e., the multiply connected part of it, we also used a novel and highly efficient algorithm for identifying the backbone. In what follows we describe these algorithms.

III. SIMULATION ALGORITHM

In the conventional simulation of IP [1,10–12] the search for the trapped regions is done after every invasion event using a Hoshen-Kopelman algorithm [2,3], which traverses the entire lattice, labels all the connected regions, and then only those sites (bonds) that are connected to the outlet face are considered as potential invasion sites (bonds). A second sweep of the lattice is then done to determine which of the potential sites (bonds) is to be invaded in the next time step. Thus, each invasion event demands $O(N^2)$ calculations, where N is the number of sites (bonds) in the lattice. This is highly inefficient for two reasons. First, after each invasion event only a small local change is made in the interface; implementing the global Hoshen-Kopelman search is unnecessary. Second, it is wasteful to traverse the entire lattice at each time step to find the most favorable site (bond) on the interface since the interface is largely static. We tackle the first problem [20,37] by searching the neighbors of each newly invaded site (bond) to check for trapping. This is ruled out in almost all instances. If trapping is possible, then several simultaneous breadth first ''forest-fire'' searches are used to update the cluster labelling as necessary [38]. This restricts the changes to the most local region possible. Since each site (bond) can be invaded or trapped at most once during an invasion, this part of the algorithm scales as $O(N)$. This cluster searching method has some similarities with the ''perimeter scouting'' algorithm for 2D clusters. In this algorithm one checks whether the most recently invaded sites could have been trapped in the interior of the cluster. If so, oriented walks are started on the just invaded site, pointing away from it to the neighboring sites, which are those that neither belong to the cluster nor are candidates for invasion. The walks continue until all but one of them have again reached the site of origin. The growth sites visited by these walks are then eliminated from the list of active sites [39]. This method is effective in 2D but not as efficient in 3D. Our method differs from it by searching cluster volumes rather than perimeters, and incorporating local checking to mini-

mize cluster searching and is thus equally effective in 3D.

The second problem is solved by storing the sites (bonds) on the fluid-fluid interface in a list, sorted according to the capillary pressure threshold (or size) needed to invade them. This list is implemented via a balanced binary search tree, so that insertion and deletion operations on the list can be performed in $\ln(n)$ time, where n is the list size. The sites (bonds) that are designated as trapped using the procedures described above are removed from the invasion list. Each site (bond) is added and removed from the interface list at most once, limiting the cost of this part of the algorithm to $O(N\ln(n))$. Thus, the execution time for N sites (bonds) is dominated (for large N) by list manipulation and scales at most as $O(N\ln(N))$ [40].

While the execution time is approximately $O(N\ln(n))$, in practice the time and memory requirements depend on the total number of lattice sites (bonds) and those forming the cluster boundary. For example, we find empirically that for 3D TIP the execution time scales as $L^{1.24}$, and the memory use is 20 bytes for each lattice site plus 64 bytes for each cluster site. On a 500 MHz 21164A Alpha microprocessor, a trapping cluster of 2×10^5 sites is grown on a $181\times181\times181$ lattice in 12.0 sec, using 120 Mbytes of memory, while in 2D a cluster of 5×10^5 sites is grown on a 2000×2000 lattice in 12.0 sec, using only 52 Mbytes. We used $L^{d-1}\times2L$ lattices in d dimensions with reflecting boundary conditions on the edges. Cluster properties were measured within the central L^d region.

We have also used a new optimized algorithm to identify the minimal path length, the sites comprising both the elastic backbone [41], i.e., the set of the sites that lie on the union of all the shortest paths between two widely separated points, and the usual transport backbone, so that the backbone search and computations do not affect the overall execution time of the algorithm. In the past, numerous algorithms have been proposed in the literature [41–44], some of which are either too slow or limited to 2D systems. For example, a recent method [45] that uses a matching algorithm takes longer to identify the backbone than the IP algorithm used here takes to generate it.

An alternative method was recently presented by Babalievski [38], based on depth-first searching out from the elastic backbone [41] to identify loops of occupied sites. This method works well for low-connectivity clusters but loses efficiency where the SSC is composed of large well-connected regions, as happens in IP with long-range correlations studied here (see below). In the latter case, some sites need to be visited numerous times before their status is decided. The method used here is an optimization of this in which the distance on the cluster from the inlet face to each cluster site is used to guide the depth-first search. In this algorithm, there are three major steps that are as follows.

(i) Using a breadth-first search algorithm, we label each site in the cluster with its ''cluster distance'' from the inlet face, and then use this information to burn backwards from the outlet face and identify the elastic backbone. At the same time, we construct the ''branch points list''–a list of all the cluster sites that are adjacent to the elastic backbone but are not part of it. The branch points list is ordered with the sites closest to the inlet face listed first. Note that the elastic backbone sites are part of the backbone.

(ii) We stop if the branch points list is empty. Otherwise, we perform a depth-first search from the last site in the branch points list, flagging all the sites that are visited. During the search, unexplored branch points are added to the branch points list, while another list tracks the sites that have been flagged as visited. We then perform an important optimization during the depth-first search: If there are multiple branches from a single site, the site labeled as being closest to the inlet face is always the first to be explored.

(iii) The depth-first search terminates when one of two conditions are satisfied: (1) the search contacts the backbone again at a different site from whence it started, in which case the sites in the visited-sites list are flagged as backbone sites, or (2) it retreats back to its starting site, at which point there will be no sites left in the visited-sites list.

(iv) The algorithm continues at step (ii).

In this way the elastic backbone, the transport backbone, and the dangling ends of the SSC are all identified. Examples of execution times for this algorithm running in 3D on a 533 MHz 21164A Alpha processor are 0.02 and 0.12 CPU sec for 32^3 and 64^3 lattices, respectively. The cluster on which these calculations were performed was a SSC generated by a NTIP. When compared with the timings reported in Ref. [45] on an equivalent hardware, our algorithm is faster by a factor of 7 for the 32^3 lattice and by a factor of 12 for a 128^3 lattice, and thus the larger the lattice size, the more efficient is our algorithm.

IV. ANALYSIS OF THE RESULTS

To estimate the various fractal dimensions, we employed two different methods. One was based on the scaling of the clusters' or paths' mass with their linear size. For example, for the SSC at the breakthrough point, i.e., when the invader first percolates through the network, we must have

$$M\propto L^{D_f}, \tag{7}$$

where M is the mass of the cluster, i.e., the number of invaded sites (bonds) in the network, L is the linear size of the sample, and D_f is the fractal dimension of the SSC. For this type of analysis, the largest lattice size that we used in 2D was $L=8192$, with the results averaged over 10^4 realizations, while in 3D we used $L=512$ and averaged the results over 5 000 realizations.

The second method of analyzing the data is based on studying the *local* fractal dimensions and their approach to their asymptotic value as M becomes very large. For example, for the SSC the local fractal dimension $D_f(M)$ is defined as

$$D_f(M)\equiv\frac{d\ln M}{d\ln R_g}, \tag{8}$$

where R_g is the cluster's radius of gyration. According to finite-size scaling theory (FSST), $D_f(M)$ converges to its asymptotic value for large M according to

$$|D_f-D_f(M)|\propto M^{-\omega}, \tag{9}$$

where ω is *a priori* unknown correction-to-scaling exponent, and thus it must be estimated from the data. Moreover, ω

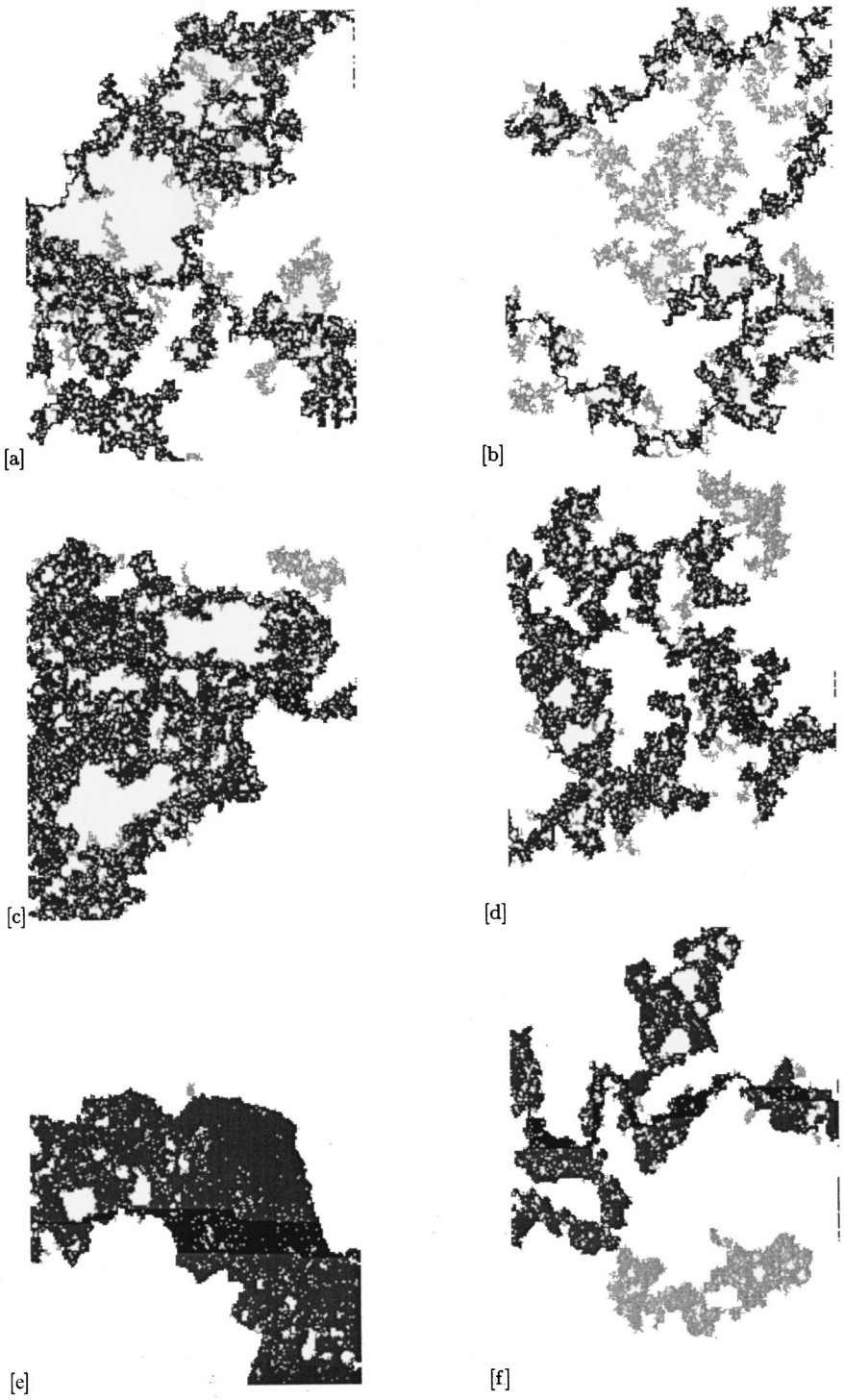

FIG. 1. Typical cluster configurations for site TIP in 2D. The results are for, from top to bottom, $H=0.2$, 0.5, and 0.9. The figures on the left show the results for a cutoff length scale $\ell_{co}=0$, while those on the right show the clusters for $\ell_{co}=8$. The light gray background is the sample-spanning cluster, the dark gray is its backbone, and the black area shows the minimal paths.

may depend on the model that we study and the quantity we estimate. Combining Eqs. (8) and (9) (and taking $R_g \propto L$) gives a differential equation that can be solved analytically. The solution is given by

$$c_1 + D_f M^{\omega} = c_2 L^{\omega D_f}, \tag{10}$$

where c_1 and c_2 are constants. Equation (10) is new and is given here for the first time. We then fit the data to Eq. (10) to estimate *both* D_f *and* ω *simultaneously*. By so doing we also avoid statistical pitfalls of the two-stage process used by Schwarzer *et al.* [17] in which the data are first divided into various bins and $D_f(M)$ are estimated by numerical differentiation, and then ω is varied until Eq. (9) provides the ''best'' straight line fit of the data when $D_f(M)$ is plotted vs $M^{-\omega}$. Note that the choice of ω is very crucial to accurate estimation of the fractal dimensions. In addition, we also

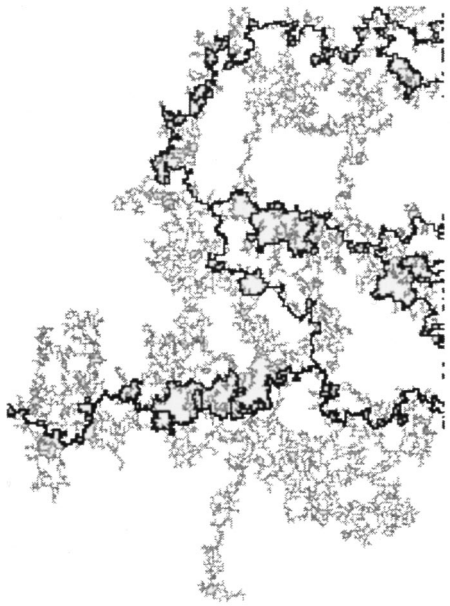

FIG. 2. Typical cluster configurations for site TIP in 2D but without any correlations. The colors are the same as in Fig. 1.

obtain reliable estimates for the confidence intervals of the model parameters, as discussed below. For this type of analysis, the 2D results were averaged over 250 000 realizations, while in 3D the results were averaged over 10^5 realizations.

V. RESULTS AND DISCUSSION

We first discuss our results in 2D, after which the results in 3D are presented and discussed.

A. Results in two dimensions

Figure 1 shows the configurations of the SSC at the breakthrough point in the site TIP model, its backbone, and the minimal path for three values of the Hurst exponent H. For the sake of comparison, we present in Fig. 2 the configuration of the SSC for site TIP without any correlations (i.e., $\ell_{co}=0$). Figure 1 shows the results for two distinct cases. In one a cutoff length scale $\ell_{co}=8$ has been introduced for the extent of the correlations, while in the second case $\ell_{co}=\infty$, i.e., the extent of the correlations is as large as the linear size of the system. As can be seen in Fig. 1, as H increases, the compactness of the SSC and its backbone also increases. For $H=0.9$ the SSC and its backbone are completely compact, with very small trapped clusters in their interior. However, when the cutoff length scale ℓ_{co} is introduced in the system, the shapes of the clusters change drastically. While at length scale $\ell<\ell_{co}$ the clusters are still compact, for $\ell>\ell_{co}$ they no longer have a compact structure. Instead, they are fractal objects with fractal dimensions that are strictly less than 2 (see below). Interestingly, although the cutoff thickens the invading front, local trapping still occurs while the fluid is advancing. Note that for $H>1/2$ the minimal path is not unique: while one can fix its length, one finds many such paths with the same length, which is why the set of all the minimal paths with a fixed length is a thick band [see Figs. 1(e) and 1(f)].

Since the fractal dimensions D_f and D_b of the SSC and its backbone in d dimensions are given by $D_f=d-\beta/\nu$ and $D_b=d-\beta_b/\nu$, where ν is the correlation length exponent and β and β_b are the critical exponents that characterize the fraction of the invaded sites in the SSC and its backbone, the compactness of these clusters implies that either $\nu=\infty$ or $\beta=\beta_b=0$ (or both), both of which imply that the percolation transition at the breakthrough point, both in the SSC and its backbone, is *first order*, in contrast with RP, uncorrelated IP, and also the SP models with long-range correlations in which the correlation function $C(r)$ decreases with increasing r [22–24], in all of which the transition at the percolation threshold is second order. Our results are similar to those of Sahimi and Mukhopadhyay [32] who reported that the SSC and its backbone for the SP model with FBM-generated correlation are compact for $H>1/2$. Isichenko [46] presented an analytical argument that indicated that, for SP and *any* $0<H<1$ in 2D, $D_f=2$.

For $H=0.5$ the SSC and its backbone appear to have started taking on a noncompact shape, with the sizes of the trapped clusters becoming much larger than those for the $H=0.9$ case. If we introduce the cutoff length scale $\ell_{co}=8$, then the trapped clusters become even larger, and for $\ell>\ell_{co}$ the clusters are again fractal objects. For $H=0.2$ the SSC and its backbone are fractal objects, with or without the cutoff length scale ℓ_{co}, although the fractal dimension D_{min} of the minimal path still deviates little from unity. Note that, in all the cases values of the fractal dimensions for the SSC and its backbone with and without the cutoff length scale are different. While for the case of no cutoff D_f and D_b (for $H<1/2$) depend on H, with the cutoff length scale these fractal dimensions are, at large length scales, the same as those of 2D site TIP without correlations. These are confirmed by our numerical analysis described below. We note that, even for $0<H<1/2$ the fractal dimension D_{min} of the minimal paths appears to be only slightly larger than unity. For example, even for $H=0.2$ shown in Fig. 1, the path seems to be almost a straight line.

Therefore, for site TIP, if there is no cutoff length scale for the extent of the correlations, then $H=1/2$ appears to signal a transition from a system with nonfractal clusters ($H>1/2$) to one with fractal clusters ($H<1/2$). Moreover, for $H<1/2$ all the fractal dimensions depend on H (see below).

The results for bond TIP are different from those for site TIP. Figure 3 presents the configurations of the SSC, its backbone, and the minimal paths for bond TIP for the same values of the Hurst exponents H and the cutoff length scale ℓ_{co} as those in Fig. 1, while Fig. 4 shows the same clusters for the same model but without any correlations (i.e., $\ell_{co}=0$). It is clear that the configurations of the clusters in the two models are completely different. In particular, the backbone of bond TIP does not contain any closed loops and is in the form of a long strand, which is in striking contrast with the backbone of site TIP that is compact for $H>1/2$, and while it is a fractal object for $H<1/2$, its fractal dimension is still quite large (see below). However, although the backbone of bond TIP is loopless and looks like a long strand, as our analysis discussed below indicates, its fractal dimension $D_{\ell b}$ is always greater than one for *any* value of H. A comparison of Figs. 2 and 4 also indicates that, even in the case

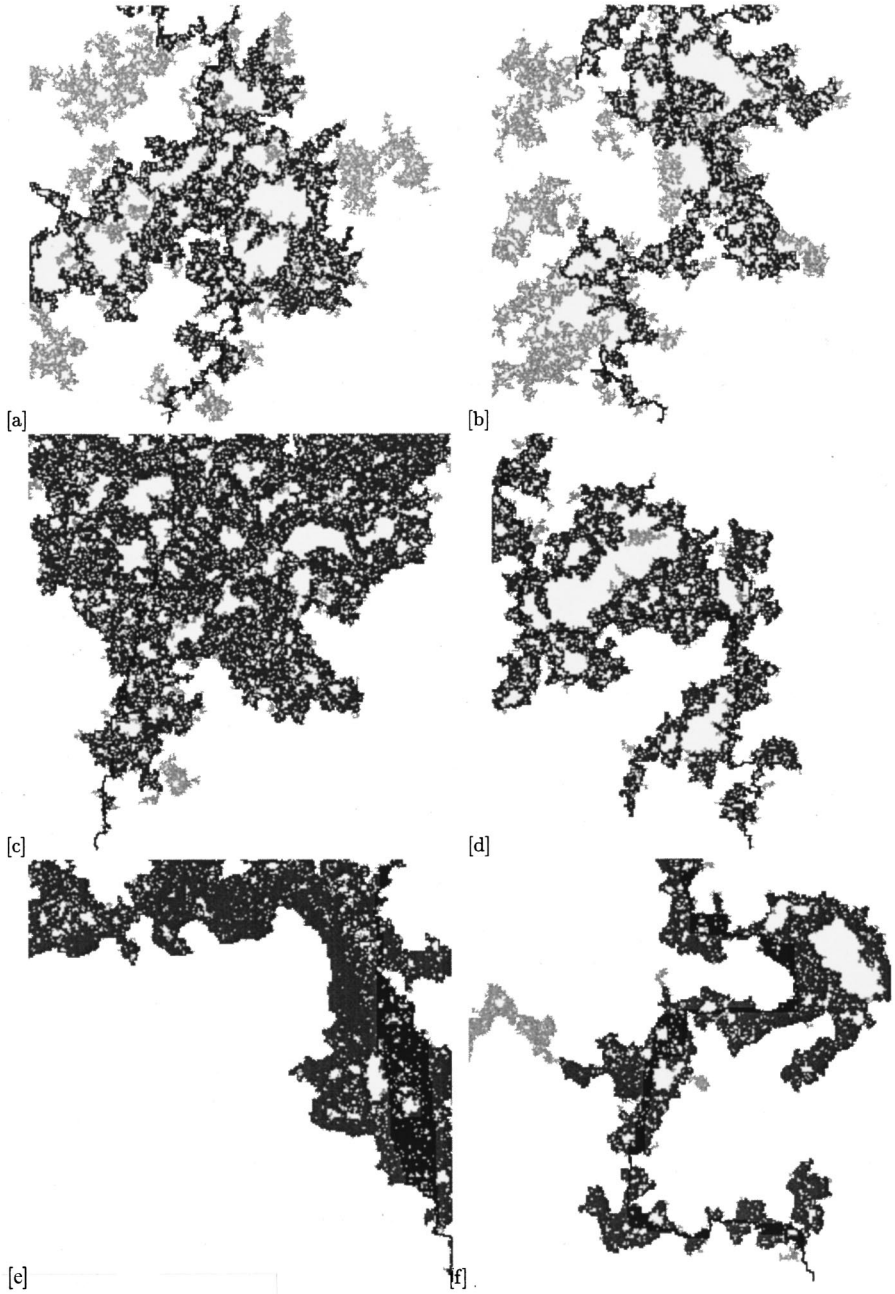

FIG. 3. Same as in Fig. 1, but for bond TIP.

of no correlations, the structures of the clusters for bond and site TIP are very different, which has also been reported previously [13,14,18,20].

We now present the analysis of our numerical results and the resulting fractal dimensions for the various clusters. Since for $H>1/2$ all the clusters are nonfractal, we discuss the results only for $H<1/2$. Figure 5 presents typical results for the mass of the clusters for $H=0.1$ and their analysis using Eq. (7). They exhibit precise scaling behavior over three orders of magnitude variations in L. The top two curves in Fig. 5 present the results for the SSC and its backbone in site TIP. For $H=0.1$ Fig. 5 yields $D_f \simeq 1.85$, while for the backbone, $D_b \simeq 1.8$, slightly smaller than D_f. The fractal dimension $D_{/b}$ of the loopless backbone of bond TIP is much smaller than D_f and D_b and for $H=0.1$ shown in Fig. 5 we find that $D_{/b} \simeq 1.16$. Figure 5 also yields $D_{min} \simeq 1.08$, only

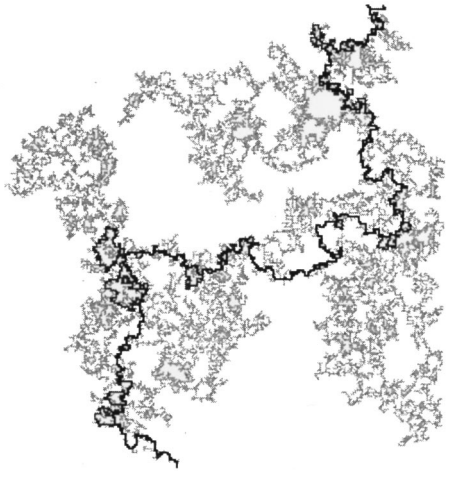

FIG. 4. Same as in Fig. 2, but for bond TIP.

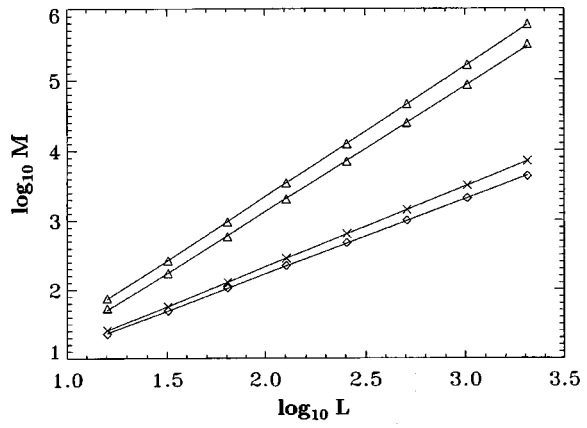

FIG. 5. Scaling of the mass M of the clusters with the length scale L for 2D TIP with $H=0.1$. The results are, from top to bottom, for the sample-spanning cluster of site TIP, the backbone of site TIP, the backbone of bond TIP, and the minimal paths for site TIP.

slightly larger than $D_{min}=1.0$ for a straight nonfractal line.

To obtain more precise estimates of the fractal dimensions, we used Eq. (10) and reanalyzed the data. Figure 6 shows typical results for the SSC in site TIP for $H=0.1$. The top figure shows the results of fitting Eq. (10) to the simulation data. The fit is effectively perfect and much more accurate than what can be attained with a simple power law, Eq. (7). In fact, one cannot distinguish the fitted results from the actual simulation results. This is perhaps not totally surprising since four parameters have been used to fit the data. The bottom figure shows the confidence region ellipse [47] of the fitting parameters ω (the FSS exponent) and D_f (the fractal dimension). The solid (dashed) line shows the 68% (99%) confidence level. It can be seen that although the confidence level for the exponent is quite broad, this does not translate into poor estimates for D_f and ω. The best fit of the data is obtained with $\omega\simeq 0.675$ and $D_f\simeq 1.8599$, slightly larger, but much more accurate, than $D_f\simeq 1.85$ obtained from Fig. 5. For comparison we show in Fig. 7 the analysis of the data using Eqs. (8) and (9), which calculates the local $D_f(M)$ numerically and then fits the results to Eq. (9) to estimate D_f and ω. This type of analysis yields $D_f\simeq 1.862$ and $\omega\simeq 0.5$. This estimate of ω is quite smaller than what we obtain from Fig. 6.

Figure 8 presents the analysis of the simulation results for the backbone in site TIP and $H=0.1$. In this case, the best fit of the data is obtained with $\omega\simeq 0.573$ and $D_b\simeq 1.8193$, distinctly lower than $D_f\simeq 1.8599$. Figure 9 depicts the results for the minimal path of site TIP for $H=0.1$, from which we estimate that $\omega\simeq 0.34$ and $D_{min}\simeq 1.0379$, not consistent with, but more accurate than, $D_{min}\simeq 1.08$ obtained from the analysis of the path's mass L (Fig. 5). Of course, the higher accuracy of the estimate obtained from Fig. 9 is due to taking into account the effect of finite-size corrections. Note that, *unlike* TIP without correlations [20], and as a consequence of the correlations, strong differences exist between the backbone and the minimal path structures. While for site TIP without correlations *local* trapping thwarts extensive growth of the backbone off the minimal path, leading to a greatly diminished backbone whose fractal dimension (see Table I) is close to that of the minimal path, for the present case the backbone is much more compact and completely different from the minimal paths.

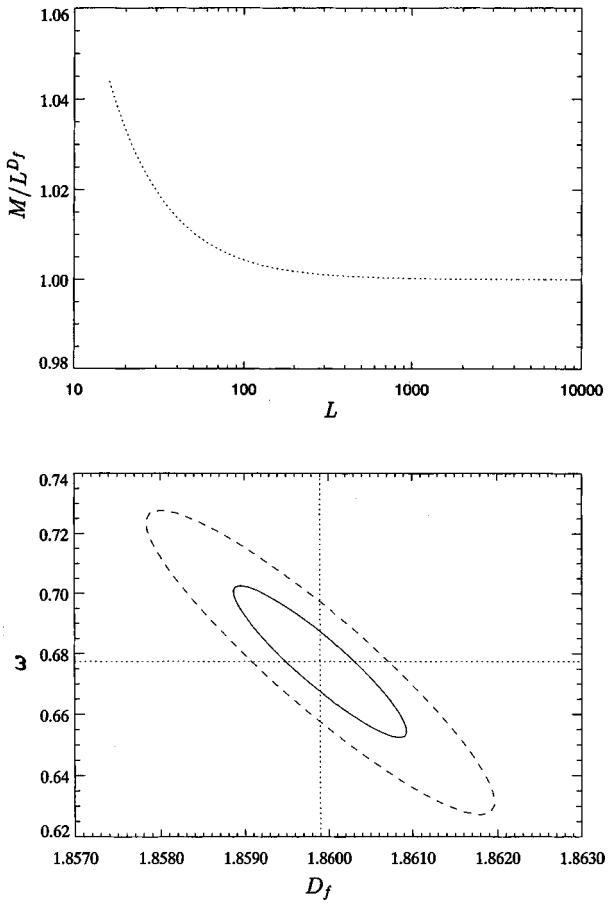

FIG. 6. Top: Fit of the simulation results for the mass of the sample-spanning cluster of 2D site TIP to Eq. (10) for $H=0.1$. The data and the fit are indistinguishable. Bottom: Confidence ellipse for the finite-size scaling exponent ω and the fractal dimension of the cluster. The solid (dashed) curve shows 68% (90%) confidence level.

Figure 10 shows typical results for the backbone of bond TIP and $H=0.1$. Confirming the qualitative features of Fig.

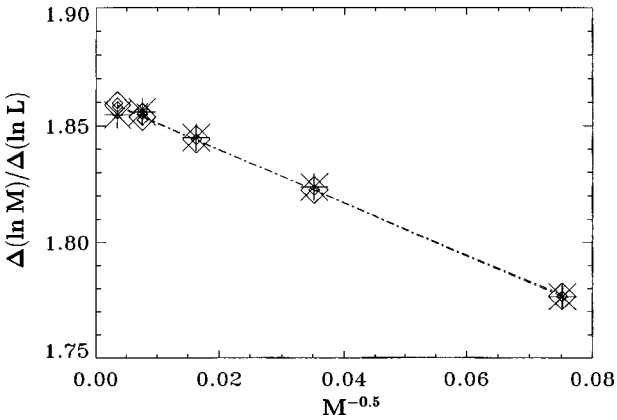

FIG. 7. Numerical analysis of the simulation results for the mass M of the sample-spanning cluster of 2D site TIP for $H=0.1$, using Eqs. (8) and (9). Large symbols are the data, while the small ones are plus and minus one standard deviation in the data.

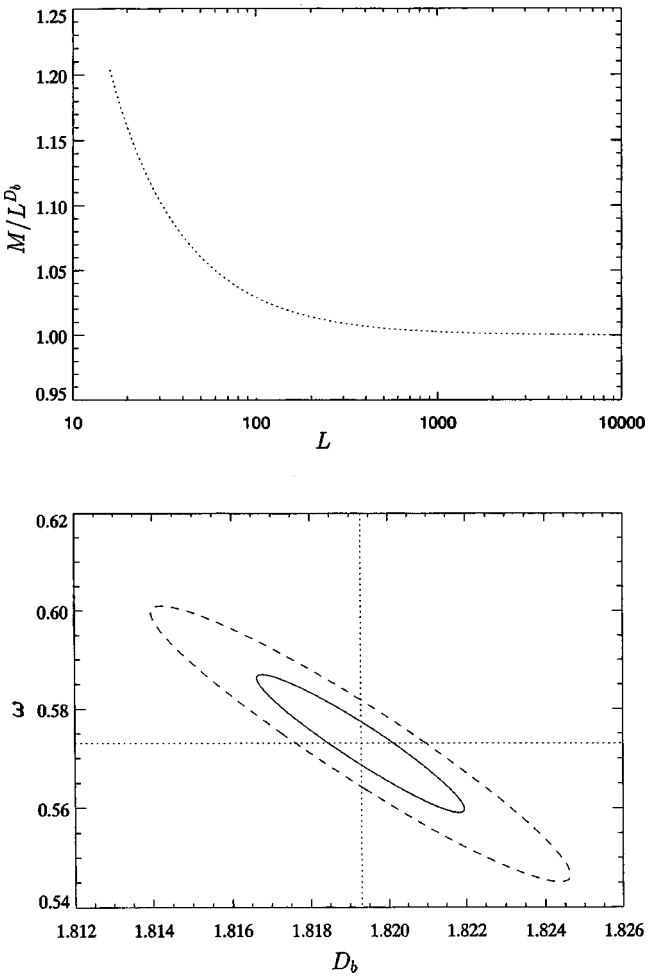

FIG. 8. Same as in Fig. 6, but for the backbone.

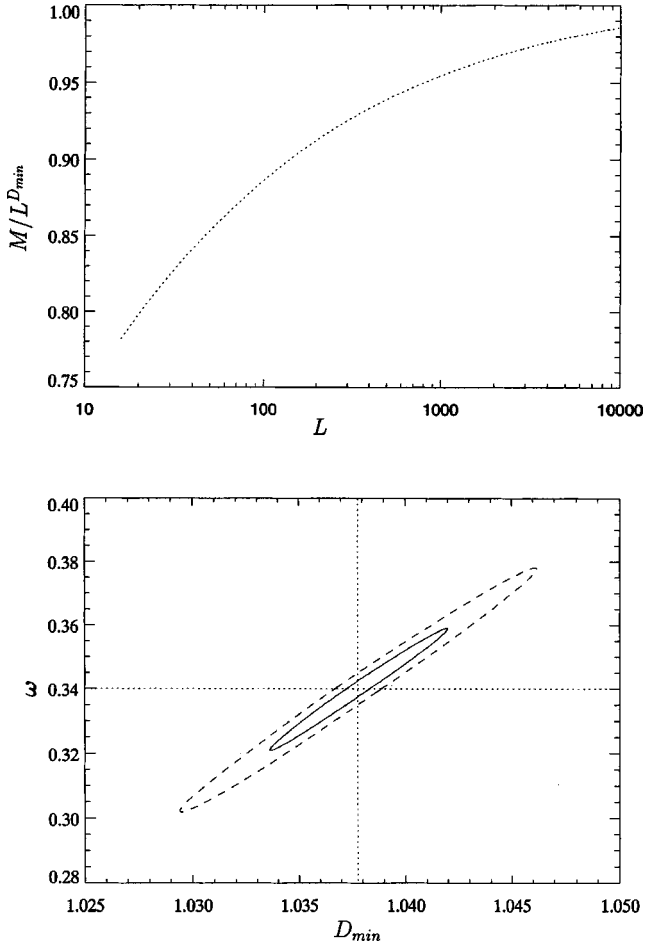

FIG. 9. Same as in Fig. 6, but for the minimum path.

3, the backbone of this model is completely different from that of site TIP. Indeed, as mentioned above, the backbone of bond TIP does not contain any closed loops of the invaded bonds and is somewhat similar to a long strand. From this figure we obtain $D_{\ell_b} \simeq 1.16$ and $\omega \simeq 0.975$. We emphasize that, had we used Eqs. (8) and (9), the estimates of these fractal dimensions, and especially their corresponding value of ω, would have been quite different. For example, for the backbone of TIP with $H=0.1$, we would have obtained $\omega \simeq 0.7$, much lower than $\omega \simeq 0.975$ that Fig. 10 yields.

To show that for $H>0.5$ the SSC (and its backbone) are compact, we present in Fig. 11 the results for $H=0.9$. As before, we obtain an excellent fit of the data (top figure), and $D_f \simeq 1.991$ and $\omega \simeq 0.41$, which confirm our assertion.

Summarizing the results in 2D, we find that for *any* value of H and a finite cutoff length scale ℓ_{co} for the extent of the correlations, all the clusters of interest are fractal at length scales $\ell > \ell_{co}$ with fractal dimensions that are the same as those of the same clusters in the corresponding IP models without any correlations. For length scales $\ell < \ell_{co}$ the clusters' structures are similar to those for $\ell_{co}=\infty$. In this case we find that for $H>1/2$ the SSC and its backbone in site TIP are compact, and that the minimal path is a straight (nonfractal) line. Moreover, we find that for *any* $H<1/2$ all the clusters of interest are fractal, but with two major differences with the case of IP without any correlations. One is that the fractal dimension D_{min} of the minimal path varies very little with H and is only slightly larger than one. The second difference is that values of all the fractal dimensions depend on H, whereas for the case of IP without correlations they are universal. Figure 12 summarizes the dependence on the Hurst exponent H of the fractal dimensions. For comparison we compile in Table I the most recent estimates of the same fractal dimensions for NTIP and TIP without correlations [20]. Finally, as was mentioned in Sec. IV, the correction-to-scaling exponent ω is a model-dependent quantity that depends on both the particular fractal dimension (or cluster) of

TABLE I. The most accurate estimates of various fractal dimensions for IP in 2D and 3D, and their comparison with those of random percolation (RP) [20].

Model	D_{min}	D_b
	2D	
NTIP	1.1293 ± 0.0010	1.6422 ± 0.0040
Site TIP	1.203 ± 0.001	1.217 ± 0.020
Bond TIP	1.2170 ± 0.0007	1.217 ± 0.0008
RP	1.1307 ± 0.0004	1.6432 ± 0.0008
	3D	
Site NTIP	1.3697 ± 0.0005	1.868 ± 0.010
Site TIP	1.3697 ± 0.0005	1.861 ± 0.005
Bond TIP	1.458 ± 0.008	1.458 ± 0.008
RP	1.374 ± 0.004	1.87 ± 0.03

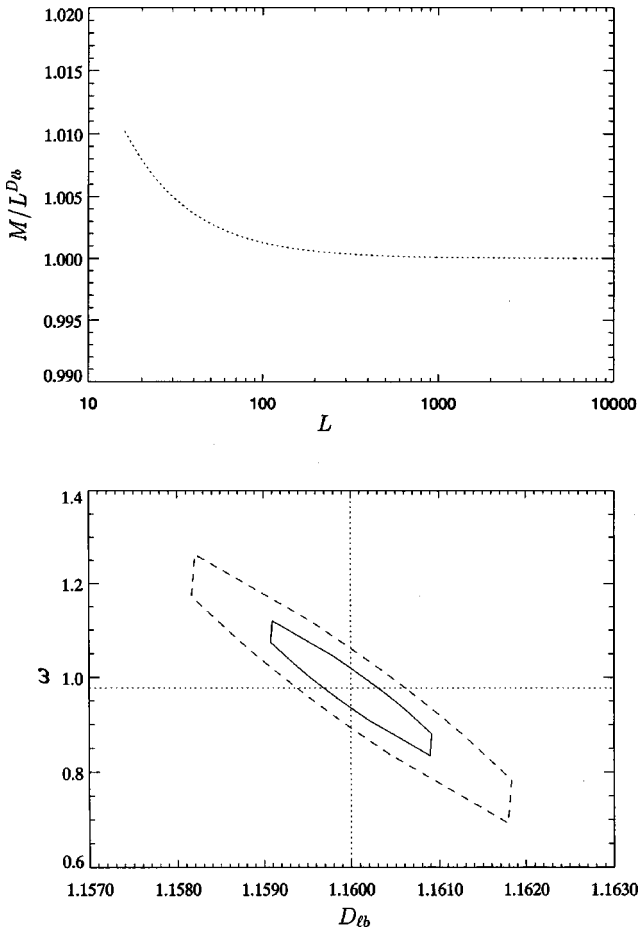

FIG. 10. Same as in Fig. 6, but for the backbone of bond TIP.

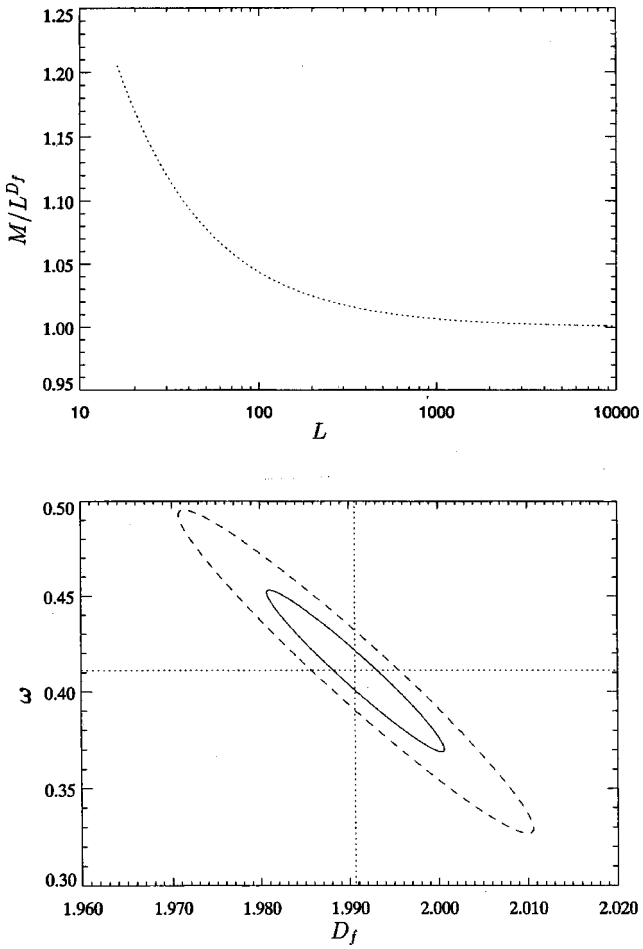

FIG. 11. Same as in Fig. 6, but for $H=0.9$.

interest to be estimated and also on the Hurst exponent H. Figure 13 presents the dependence of ω on H for the four fractal dimensions.

B. Results in three dimensions

Similar to the 2D case, we find that in 3D all the clusters are compact for $H>1/2$. Therefore, once again $H=1/2$ represents a sort of transition point from compact (for $H>1/2$) to fractal clusters (for $H<1/2$). However, we find that there are significant qualitative differences between the structure of the various clusters, which we now discuss.

We first consider the fractal structure of the clusters. To make a direct comparison with Figs. 5–10, we present the typical results for $H=0.1$. Figure 14 presents the analysis of the clusters' masses according to Eq. (7). From the best fit of the data we obtain $D_f \simeq 2.72 \pm 0.01$, practically identical with $D_b \simeq 2.71 \pm 0.01$. We also find that $D_{\not\ell} \simeq 1.29 \pm 0.01$ and $D_{min} \simeq 1.09 \pm 0.02$. These results indicate that (1) the SSC and its backbone are practically identical, which is a surprising result, and (2) similar to 2D, the fractal dimension D_{min} of the minimal path is very close to 1. Indeed, a closer inspection of the results indicates that Eq. (7) is not adequate enough for yielding an accurate estimate of any of the fractal dimensions.

Therefore, similar to 2D, in order to obtain more precise estimates of the fractal dimensions, we used the asymptotic analysis of the fractal dimensions using Eq. (10). Figures 15 and 16 show the results for the SSC and its backbone, respectively, from which we obtain $D_f \simeq 2.771$ ($\omega \simeq 0.52$) and $D_b \simeq 2.745$ ($\omega \simeq 0.255$). These results indicate that in 3D and for $H<1/2$ the SSC and its backbone are fractal with fractal dimensions that are nearly identical. The difference between the two fractal dimensions is *smaller* than what we found in 2D (see above) which is surprising, because one

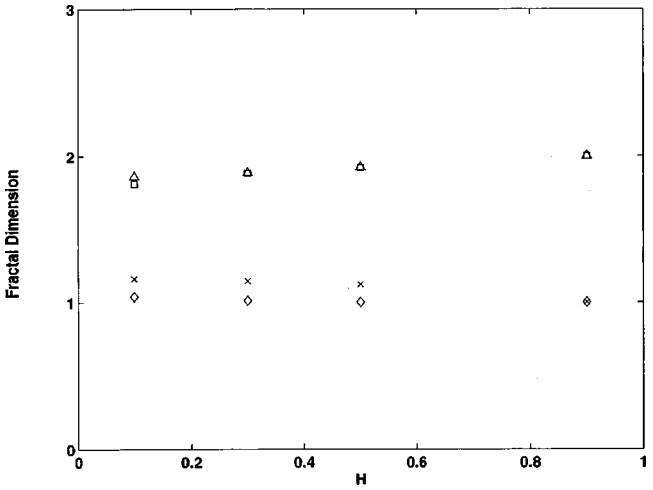

FIG. 12. Dependence of the various fractal dimensions on H for 2D TIP. The results are for the site sample-spanning cluster (triangles), site backbone (squares), backbone of bond TIP (crosses), and site minimal paths (diamonds).

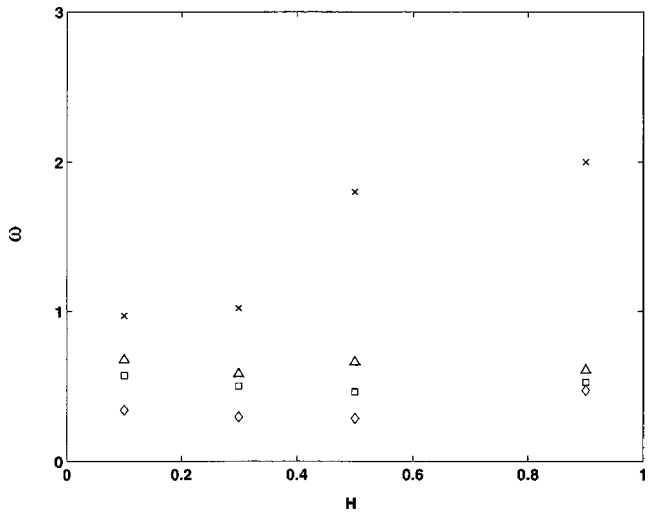

FIG. 13. Dependence of the finite-size scaling exponent ω on H in 2D. Symbols are the same as in Fig. 12.

would intuitively think that the probability that some regions of the SSC to be deadends off the backbone is much higher in 3D than in 2D. In their study of standard percolation with long-range correlations that were generated by the FBM, Sahimi and Mukhopadhyay [32] also reported that the SSC and its backbone are very similar, although due to the small lattice sizes that they used, they could not quantify the similarity between the SSC and its backbone.

Figure 17 presents the results for the minimal path. In this case we obtain $D_{min} \simeq 0.985$ ($\omega \simeq 0.21$), indicating strongly that, in 3D the minimal path is *not* fractal for *any* H. Recall that we found in 2D that the fractal dimension D_{min} is only slightly larger than 1. Therefore, it is possible that the same is true in 2D, namely, that the asymptotic (very large L) value of fractal dimension D_{min} is 1, but one must use very large lattices in order to reach this asymptotic value.

Figure 18 shows the results for the backbone of bond TIP, which is loopless, from which we obtain $D_b \simeq 1.303$ and $\omega \simeq 0.0$. Note that, as the top figure indicates, in this case the asymptotic regime is reached for $L \simeq 40$, indicating very fast convergence to the true value.

Since for $H < 1/2$ the fractal dimensions D_f, D_b, and D_ℓ depend on H, we have calculated their values for a few values of H. The results are summarized in Fig. 19. Moreover, similar to 2D, the exponent ω also depends on the cluster studied and also on H. Thus, we present in Fig. 20 the dependence of ω on H for the three cluster structures studied.

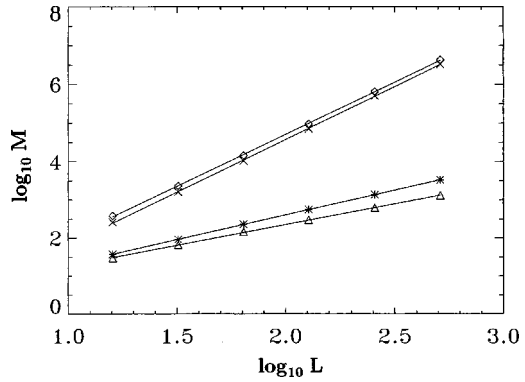

FIG. 14. Scaling of the mass M of the clusters with the length scale L for 3D TIP with $H = 0.1$. The results are, from top to bottom, for site sample-spanning cluster, site backbone, backbone of bond TIP, and site minimal paths.

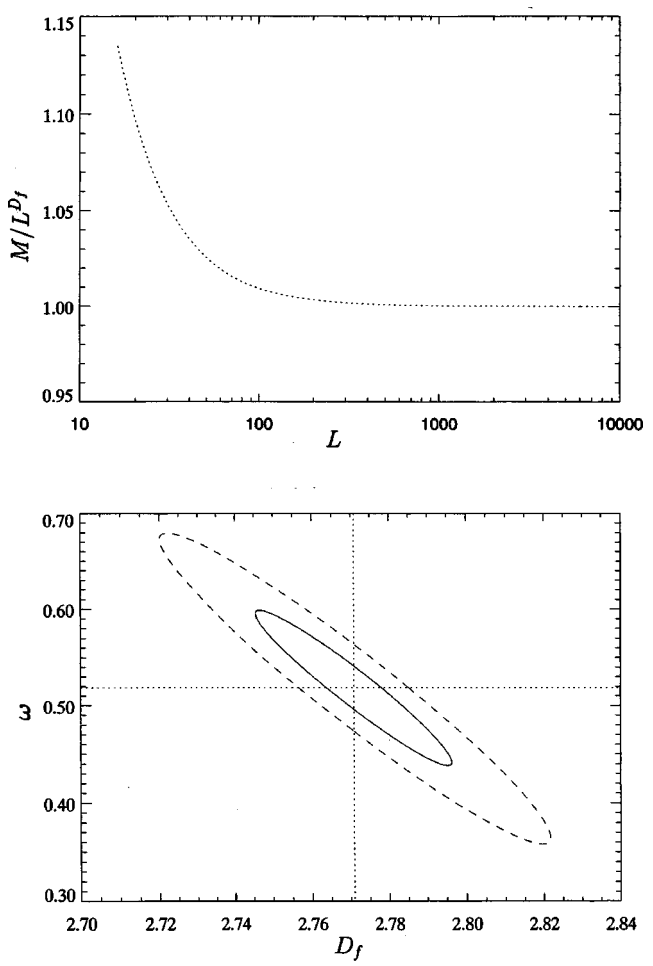

FIG. 15. Same as in Fig. 6, but in 3D.

As discussed above, since we have introduced a cutoff length scale ℓ_{co}, one should see a clear crossover from a value of the fractal dimension for length scales $\ell \gg \ell_{co}$ that corresponds to that of TIP without any correlations, to a compact cluster for $H > 0.5$, or to an H-dependent fractal dimension for $H < 0.5$, for $\ell < \ell_{co}$. Figure 21 shows this analysis for the 2D backbone of TIP with $H = 0.9$ and $\ell_{co} = 256$. The crossover is clearly evident. The slope of the plot at short length scales is $D_b = 2$, indicating a compact backbone, while at large length scales there is a crossover to $D_b < 2$, confirming what we asserted above.

C. Size distribution of the trapped clusters

Another important topological property of percolation networks is the average number of clusters of size s. In IP the invader grows only in a single cluster along a path of least resistance. Therefore, at the breakthrough the invader forms no disconnected clusters. However, for IP with trapping, one can continue the invasion process beyond the breakthrough point to a second percolation threshold at which the defending phase consists only of isolated clusters and the invasion must cease. We consider the cluster size distribution for the trapped defender clusters on correlated lattice at this thresh-

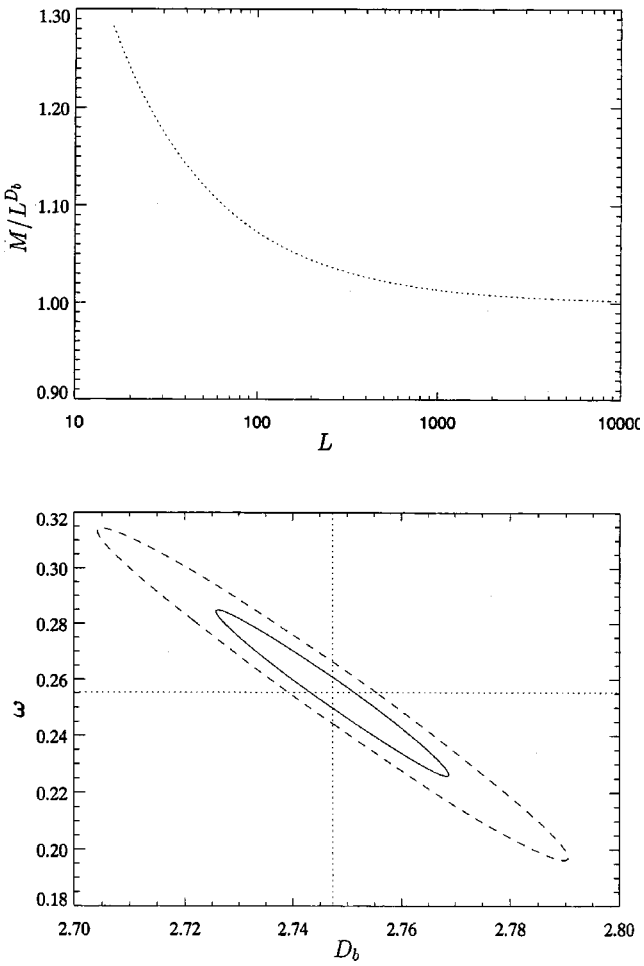

FIG. 16. Same as in Fig. 8, but in 3D.

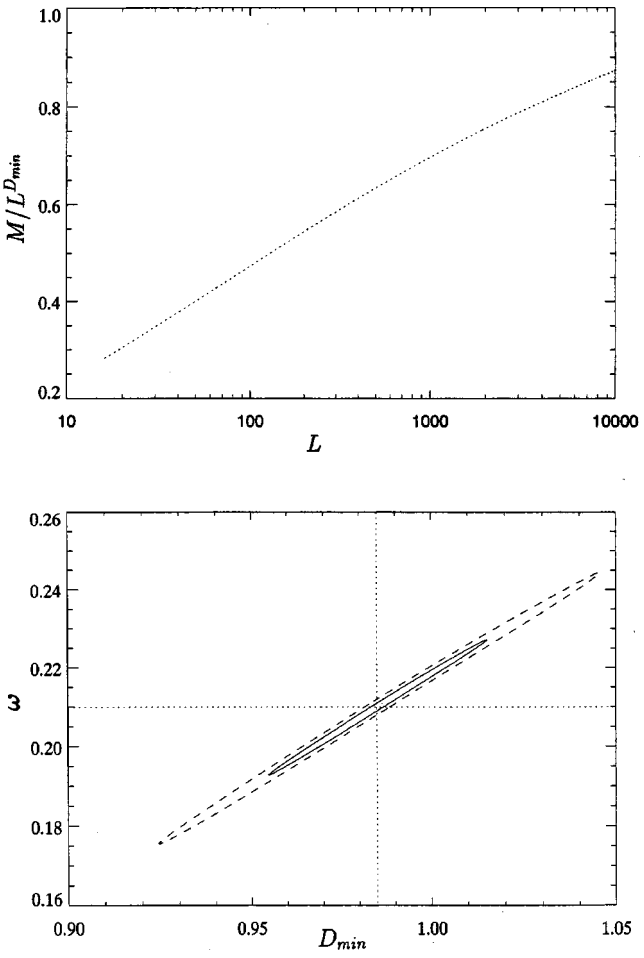

FIG. 17. Same as in Fig. 9, but in 3D.

old. Normally, one studies $n_s(s)$, the number of clusters of size s (where a cluster's size is simply the total number of sites that it contains). In general, one expects to have

$$n_s(s) \sim s^{-\tau} f(s/\langle s \rangle), \tag{11}$$

where $f(x)$ is a scaling function, and $\langle s \rangle$ is the mean cluster size, defined by

$$\langle s \rangle = \frac{\sum_s s^2 n_s(s)}{\sum_s s n_s(s)}. \tag{12}$$

However, because of large variations of the clusters' configurations among different realizations, a more accurate way of studying the cluster size statistics is [48] by investigating $N_s(s) = \Sigma_{s>} s n_s$, the average total number of clusters with a size greater than a given size s. In general one expects to have

$$N_s(s) \propto s^{2-\tau}. \tag{13}$$

If there are no long-range correlations in the system, then the exponent τ is universal. Since the 3D SSC for both site and bond TIP with no long-range correlations has the same fractal dimension as RP, then for this case, $\tau = d/D_f + 1 \simeq 2.19$, so that in a logarithmic plot of $N_s(s)$ vs s the slope of the straight line would be $2 - \tau \simeq -0.19$. For the present correlated cases, however, we have two distinct regimes. (1) For $H > 1/2$ the SSC is compact, and we do not expect to have a scaling law similar to (11) or (13). (2) For $H < 1/2$ the SSC is a fractal object, and therefore a scaling law similar to (11) or (13) should hold except that, since D_f is nonuniversal and depends on H, we may expect to also have nonuniversal values of τ that depend on H. Moreover, if we introduce a cutoff length scale ℓ_{co} for the extent of the correlations, then for length scales $L \gg \ell_{co}$ we expect to recover the behavior with no correlations, whereas for $L \ll \ell_{co}$ we should have one of the above two cases, depending on the value of H.

To check this, we have studied the scaling of $N_s(s)$ for various values of H and the cutoff length scale ℓ_{co}. Shown in Fig. 22 is the distribution of the trapped clusters for $H = 0.2$ and various values of the cutoff length scale ℓ_{co}. As can be seen for the case of no correlations (i.e., $\ell_{co} = 0$) one obtains good agreement with the expected behavior. However, as ℓ_{co} increases, the cluster size distribution starts to deviate significantly from the random case. This behavior becomes even clearer when we study a system with $H > 1/2$, an example of which is shown in Fig. 23, where we show the results for $H = 0.8$ and various cutoff length scales. For large ℓ_{co} it is difficult to obtain any sort of scaling, which is consistent with our discussion.

These results are corroborated if we study the size of the

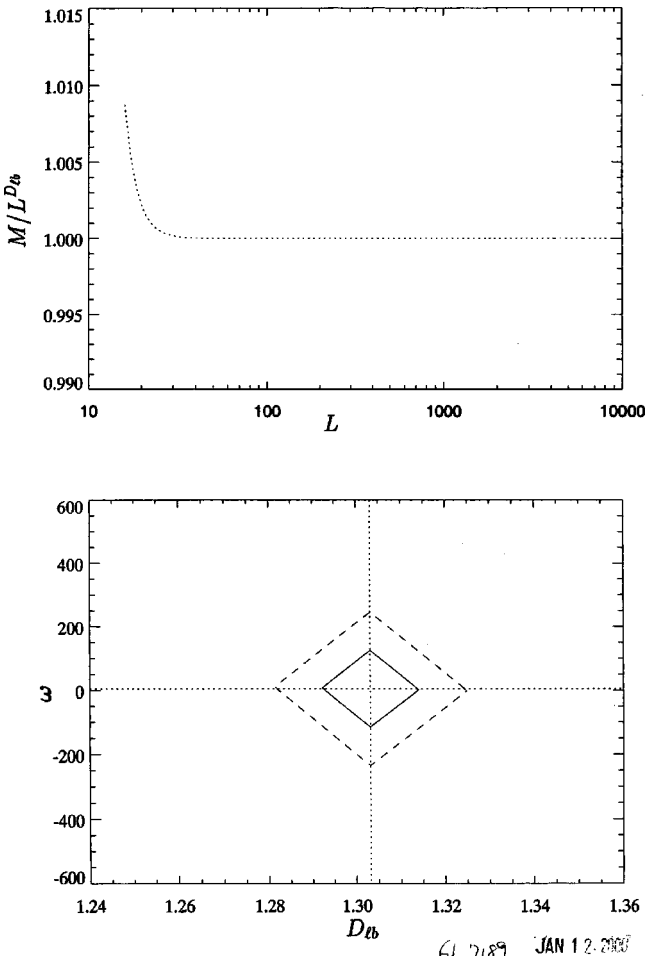

FIG. 18. Same as in Fig. 10, but in 3D.

individual trapped clusters as a function of ℓ_{co}. Our simulations indicate that for small ℓ_{co} there is only a small effect on the distribution of the trapped clusters; this is also evident in Fig. 22. For intermediate values of ℓ_{co} we observe a higher proportion of the trapped sites lie in larger trapped clusters. As $\ell_{co}\to\infty$, one single cluster contains over 30% of the trapped sites. The trapping dynamics also depends

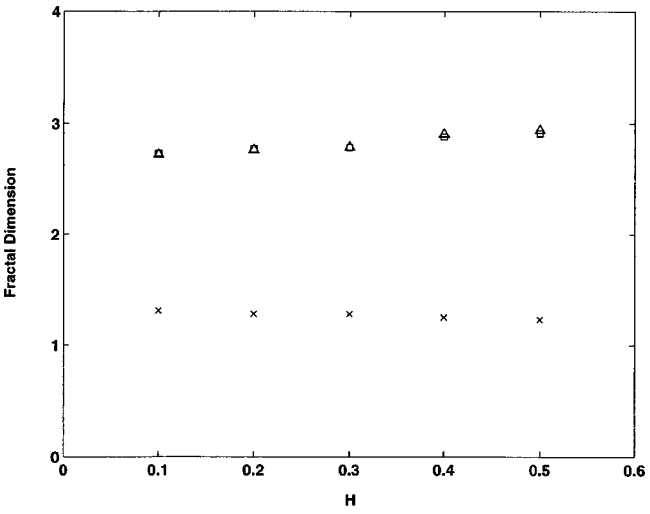

FIG. 19. Same as in Fig. 12, but in 3D.

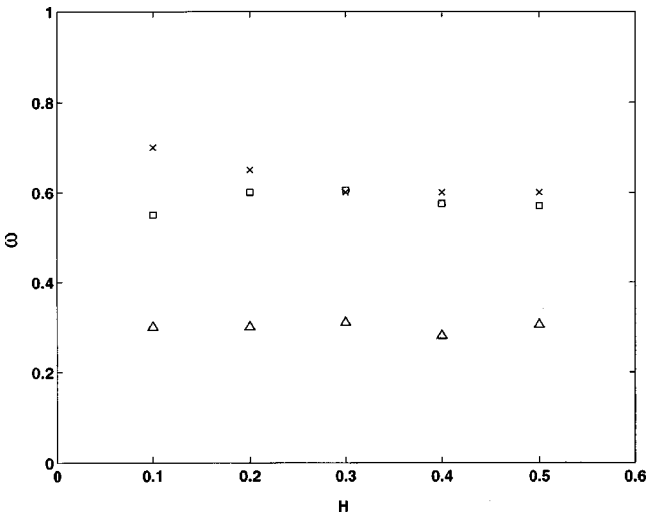

FIG. 20. Same as in Fig. 13, but in 3D.

strongly on the presence of the correlations. In a random system, trapping occurs *only* near the end of the invasion process, where over 80% of the total invading fluid is present and less than 5% of the defender is trapped. In contrast, with a cutoff length scales of, say $\ell_{co}=16$, over 30% of the defending fluid is trapped at 80% invader saturation.

VI. SUMMARY AND DISCUSSION

Using highly efficient algorithms for invasion percolation and its backbone, we have studied trapping IP with long-range correlations. The correlations are generated by a fractional Brownian motion. For Hurst exponents $H>1/2$, i.e., when the correlations are positive, the sample-spanning cluster and its backbone are compact, while for $H<1/2$, i.e., when the correlations are negative, they appear to be fractal. Therefore, $H=1/2$ signifies a sort of transition from a compact to a fractal system. Since compact clusters imply first-order phase transitions, $H=1/2$ can be interpreted as the point at which one has a crossover from a first-order phase transition (for $H>1/2$) to a second-order phase transition (for $H<1/2$). In the latter case all the fractal dimensions of the model, as well as the exponent that characterizes the

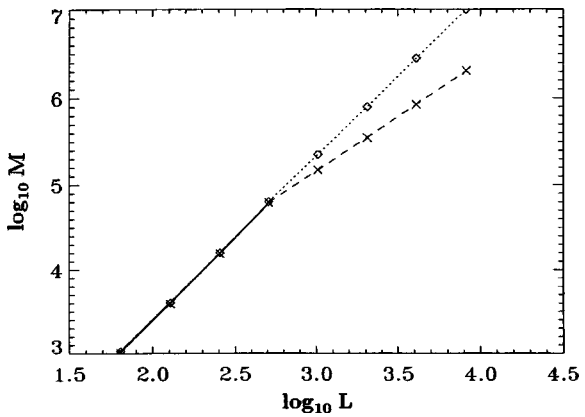

FIG. 21. Crossover from a compact backbone at small length scales (diamonds) to a fractal backbone at large length scales (crosses) for 2D site TIP with $H=0.9$. The cutoff length scale for the correlations is $\ell_{co}=256$.

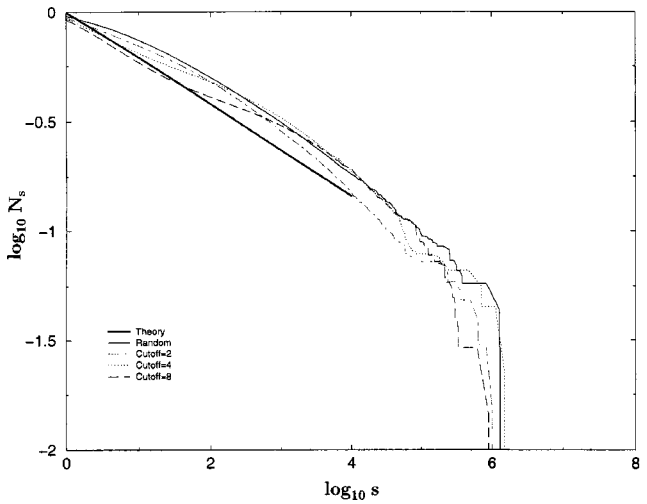

FIG. 22. Cumulative trapped cluster size distribution N_s vs the cluster size s for 3D site TIP with $H=0.2$ and $L=512$. ''Theory'' refers to random percolation.

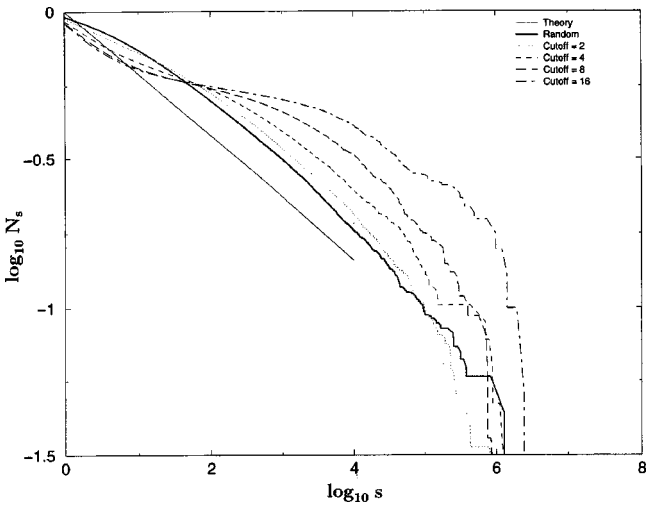

FIG. 23. Same as in Fig. 22, but for $H=0.8$.

scaling properties of its cluster size distribution, depend on the Hurst exponent H.

Thus, unlike uncorrelated 2D IP, which is characterized by two universality classes (one for IP without trapping that is the same as that of RP, and another one for bond and site TIP) [20], and the 3D model for which one has two distinct universality classes (one for site IP with or without trapping that is the same as that of RP, and one for bond TIP) [20], the present TIP model is not characterized by a finite number of universality classes, as the relevant fractal dimensions and exponents vary continuously with $H<1/2$.

Elsewhere [49] we have discussed the implications of these results for oil recovery operations and extraction of the trapped oil blobs in the reservoir.

ACKNOWLEDGMENTS

M.A.K. is grateful to the Australian Research Council for financial support. Work at USC was supported in part by the Petroleum Research Fund, administered by the American Chemical Society. We thank the staffs of the ANU Supercomputing Facility and the High Performance Computing Facility at the University of Queensland for generous allocations of computer time.

[1] M. Sahimi, Rev. Mod. Phys. **65**, 1393 (1993); *Flow and Transport in Porous Media and Fractured Rock* (VCH, Weinheim, Germany, 1995).

[2] D. Stauffer and A. Aharony, *Introduction to Percolation Theory*, 2nd ed. (Taylor and Francis, London, 1992); A. Bunde and S. Havlin, *Fractals and Disordered Systems*, 2nd ed. (Springer, Berlin, 1996).

[3] M. Sahimi, *Applications of Percolation Theory* (Taylor and Francis, London, 1994).

[4] R.G. Larson, L.E. Scriven, and H.T. Davis, Chem. Eng. Sci. **36**, 57 (1981).

[5] A.A. Heiba, M. Sahimi, L.E. Scriven, and H.T. Davis, Society of Petroleum Engineers Report No. 11015 (Society of Petroleum Engineers, Richardson, Texas, 1982); SPE Reservoir Eng. **7**, 123 (1992).

[6] A. Kantzas and I. Chatzis, Chem. Eng. Commun. **69**, 191 (1988).

[7] M. Sahimi, Chem. Eng. Commun. **64**, 179 (1988).

[8] M.J. Blunt and P.R. King, Transp. Porous Media **6**, 407 (1991); S. Bryant and M.J. Blunt, Phys. Rev. A **46**, 2004 (1992); M.J. Blunt, M.J. King, and H. Scher, *ibid.* **46**, 7680 (1992).

[9] P.A. Goode and T.S. Ramakrishnan, AIChE. J. **39**, 1124 (1993).

[10] R. Lenormand and S. Bories, C. R. Seances Acad. Sci., Ser. B **291**, 279 (1980); R. Chandler, J. Koplik, K. Lerman, and J.F. Willemsen, J. Fluid Mech. **119**, 249 (1982).

[11] D. Wilkinson and J. Willemsen, J. Phys. A **16**, 3365 (1983).

[12] L. Furuberg, J. Feder, A. Aharony, and T. Jøssang, Phys. Rev. Lett. **61**, 2117 (1988).

[13] M. Cieplak, A. Maritan, and J.R. Banavar, Phys. Rev. Lett. **72**, 2320 (1994); **76**, 3754 (1996).

[14] M. Porto, S. Havlin, S. Schwarzer, and A. Bunde, Phys. Rev. Lett. **79**, 4060 (1997).

[15] J. Machta, Y.S. Choi, A. Lucke, and T. Schweizer, Phys. Rev. Lett. **75**, 2792 (1995); G. Franzese, V. Cataudella, and A. Coniglio, Phys. Rev. E **57**, 88 (1998).

[16] C.P. Stark, Nature (London) **352**, 423 (1991); R. Cafiero, A. Gabrielli, M. Marsili, and L. Pietronero, Phys. Rev. E **54**, 1406 (1996).

[17] M. Porto, A. Bunde, S. Havlin, and H.E. Roman, Phys. Rev. E **56**, 1667 (1997); M. Porto, S. Havlin, H.E. Roman, and A. Bunde, *ibid.* **58**, 5205 (1998); S. Schwarzer, S. Havlin, and A. Bunde, *ibid.* **59**, 3262 (1999). See, P. Grassberger, J. Phys. A **32**, 6233 (1999), where a critique of these authors' method is presented.

[18] M. Sahimi, M. Hashemi, and J. Ghassemzadeh, Physica A **260**, 231 (1998).

[19] A.-L. Barabási, Phys. Rev. Lett. **76**, 3750 (1996).

[20] A.P. Sheppard, M.A. Knackstedt, W.V. Pinczewski, and M.

Sahimi, J. Phys. A **32**, L521 (1999).
[21] A. Coniglio, C. Nappi, L. Russo, and F. Peruggi, J. Phys. A **10**, 205 (1977).
[22] A. Weinrib and B.I. Halperin, Phys. Rev. B **27**, 413 (1983); A. Weinrib, *ibid.* **29**, 387 (1984).
[23] M.B. Isichenko and J. Kalda, J. Nonlinear Sci. **1**, 255 (1991).
[24] S. Prakash, S. Havlin, M. Schwartz, and H.E. Stanley, Phys. Rev. A **46**, R1724 (1992).
[25] M. Sahimi, Phys. Rep. **306**, 213 (1998).
[26] B.B. Mandelbrot and J.W. Van Ness, SIAM Rev. **10**, 422 (1968).
[27] S. Rambaldi and O. Pinazza, Physica A **208**, 21 (1994).
[28] M. Sahimi, J. Phys. I **4**, 1263 (1994); AIChE. J. **41**, 229 (1995).
[29] T.A. Hewett, Society of Petroleum Engineers Report No. 15386 (Society of Petroleum Engineers, Richardson, Texas, 1986); A. Arya, T.A. Hewett, R.G. Larson, and L.W. Lake, SPE Reservoir Eng. **3**, 139 (1988); T.A. Hewett and R.A. Behrens, SPE Form. Eval. **5**, 217 (1990); see also H.H. Hardy and R.A. Beier, *Fractals in Reservoir Engineering* (World Scientific, Singapore, 1994).
[30] S.P. Neuman, Geophys. Res. Lett. **21**, 349 (1994).
[31] J. Schmittbuhl, J.-P. Vilotte, and S. Roux, J. Phys. A **26**, 6115 (1994).
[32] M. Sahimi and S. Mukhopadhyay, Phys. Rev. E **54**, 3870 (1996).
[33] V.V. Mourzenko, J.-F. Thovert, and P.M. Adler, Phys. Rev. E **59**, 4265 (1999).
[34] G. Wagner, P. Meakin, J. Feder, and T. Jøssang, Physica A **264**, 321 (1999).
[35] M.A. Knackstedt, A.P. Sheppard, and W.V. Pinczewski, Phys. Rev. E **58**, R6923 (1998).
[36] R.F. Voss, in *Fundamental Algorithms for Computer Graphics*, edited by R.A. Earnshaw, NATO ASI Series, Vol. 17 (Springer-Verlag, Heidelberg, 1985), p. 805.
[37] A.P. Sheppard (unpublished).
[38] F. Babalievski, Int. J. Mod. Phys. C **9**, 43 (1998).
[39] P. Meakin, Physica A **173**, 305 (1991).
[40] A somewhat similar algorithm has been used by Schwarzer *et al.*, Ref. [17].
[41] H.J. Herrmann, D.C. Hong, and H.E. Stanley, J. Phys. A **17**, L261 (1984).
[42] C. Liem and N. Jan, J. Phys. A **21**, L243 (1988).
[43] M.D. Rintoul and H. Nakanishi, J. Phys. A **27**, 5445 (1994).
[44] P. Grassberger, Physica A **262**, 251 (1999).
[45] C. Moukarzel, Int. J. Mod. Phys. C **9**, 887 (1998).
[46] M.B. Isichenko, Rev. Mod. Phys. **64**, 961 (1992).
[47] W.H. Press, S.A. Teukolsky, W.T. Vetterling, and B.P. Flannery, *Numerical Recipes*, 2nd ed. (Cambridge University Press, Cambridge, 1992), Chap. 15.
[48] M.M. Dias and D. Wilkinson, J. Phys. A **19**, 3131 (1986).
[49] M.A. Knackstedt, S.J. Marrink, A.P. Sheppard, W.V. Pinczewski, and M. Sahimi, *Transport in Porous Media* (in press); M.A. Knackstedt, A.P. Sheppard, and M. Sahimi, Adv. Water Resour (to be published).